CHEMISTRY
A EUROPEAN JOURNAL

DOI: 10.1002/chem.200903263

Hierarchical Hollow Co_9S_8 Microspheres: Solvothermal Synthesis, Magnetic, Electrochemical, and Electrocatalytic Properties

Yu-Xue Zhou,[a, c] Hong-Bin Yao,[a] Yi Wang,[b] Hui-Li Liu,[a] Min-Rui Gao,[a] Pei-Kang Shen,[b] and Shu-Hong Yu*[a]

Abstract: A simple solvothermal route in a binary solution of triethylenetetramine (TETA) and deionized water (DIW) has been used to synthesize hierarchical hollow Co_9S_8 microspheres with high surface area ($80.38\ m^2\ g^{-1}$). An appropriate volume ratio of TETA:DIW has been found to be essential for the formation of hollow Co_9S_8 microspheres. The magnetic study indicated that the Co_9S_8 hollow microspheres are paramagnetic at high temperature and antiferromagnetic at low temperature. The oxygen reduction reaction experiments demonstrated that the onset potential of the Co_9S_8 sample is 0.88 V, which is comparable to the value predicted for Co_9S_8 (0.74 V) from the theoretical simulation. The discharge capability of Co_9S_8 hollow microspheres as cathode materials for lithium ion batteries and their electrocatalytic activity for the oxygen reduction reaction (ORR) have been studied.

Keywords: cobalt · electrochemistry · hierarchical structures · magnetic properties · solvothermal synthesis · sulfur

Introduction

In the past few years, hollow nano- and microspheres with well-defined architectures have aroused more and more interest due to their special properties and promising application in efficient catalysts, drug-delivery carriers, photonic crystals, water treatment, lithium ion batteries materials, and so forth.[1] Recently, template-assisted approaches have usually been employed for preparing hollow spheres by using soft templates such as vesicles,[2] emulsion droplets,[3] and gas bubbles,[4] as well as hard templates such as silica,[5] polystyrene (PS) spheres,[6] resin spheres,[7] carbon spheres,[8] and so on. However, the above two-step template synthesis procedure has some disadvantages related to its being time-consuming, and having high cost and low reproducibility, which restrains the scale-up of its industrial applications. Therefore, developing one-pot solution routes for the preparation of hollow spheres still remains a major challenge and currently much effort is being devoted to establishing template-free chemical processes, based on the Kirkendall effect,[9] Ostwald ripening,[10] chemically induced self-transformation,[11] and galvanic replacement[12] to synthesize hollow spheres in a cost-effective and high-output way.

Semiconductor transition-metal chalcogenides are of great interest because of their potential wide-ranging applications in fields such as optical sensors,[13] optoelectronic devices,[14] magnetic devices,[15] and catalysts.[16] Among a variety of transition metal sulfides, Co_9S_8 is an effective hydro-desulfurization catalyst,[17] and is found to have the highest catalytic activity for the oxygen reduction reaction (ORR) in acidic solution.[16,18] The charge and discharge capabilities of Co_9S_8[19] have already been studied, and show that Co_9S_8 is a promising cathodic material for lithium ion batteries; the study of the magnetic properties of Co_9S_8 shows the potential application of Co_9S_8 in a magnetic field.[20] Due to the important application of Co_9S_8 in various domains, Co_9S_8

[a] Dr. Y.-X. Zhou, Dr. H.-B. Yao, H.-L. Liu, Dr. M.-R. Gao, Prof. Dr. S.-H. Yu
Division of Nanomaterials and Chemistry
Hefei National Laboratory for Physical Sciences at Microscale
Department of Chemistry
National Synchrotron Radiation Laboratory
University of Science and Technology of China
Hefei, Anhui 230026 (P. R. China)
Fax: (+86) 551-3603040
E-mail: shyu@ustc.edu.cn

[b] Dr. Y. Wang, Prof. Dr. P.-K. Shen
State Key Laboratory of Optoelectronic Materials and Technologies
School of Physics and Engineering, Sun Yat-Sen University
Guangzhou 510275 (P. R. China)

[c] Dr. Y.-X. Zhou
School of Physical Science and Technology, Yangzhou University
Yangzhou, Jiangsu 225009 (P. R. China)

Supporting information for this article is available on the WWW under http://dx.doi.org/10.1002/chem.200903263.

materials have attracted more and more attention in the field of materials science. Although Co_9S_8 nanoparticles[21] and hollow Co_9S_8 nanospheres[9,22] have been fabricated and investigated recently, to the best of our knowledge, hierarchical hollow Co_9S_8 microspheres assembled by quasi-hexangular nanoplates based on template-free chemical synthesis, as well as their properties, have not been reported previously.

In this paper, hollow Co_9S_8 microspheres constructed by quasi-hexangular nanoplates have been synthesized on a large scale by a solvothermal reaction in a mixed solution system,[23] using $CoCl_2{\cdot}6H_2O$ and C_2H_5NS as raw materials. The volume ratio of triethylenetetramine (TETA) and deionized water (DIW) has a significant influence on the morphology of the product, and a certain volume ratio of TETA to DIW is essential for the formation of hollow Co_9S_8 microspheres. Their magnetic properties, discharge capability of Co_9S_8 hollow microspheres as cathode materials for lithium ion batteries, and electrocatalytic activity for oxygen reduction reaction (ORR) have been studied.

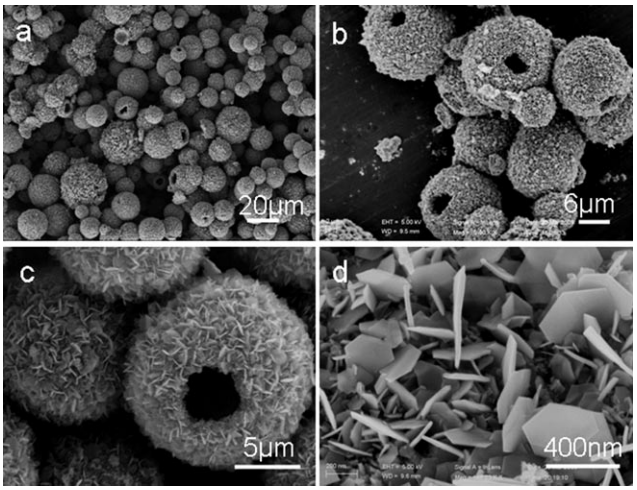

Figure 2. FESEM images of Co_9S_8 hollow microspheres prepared by a solvothermal reaction in a mixed solvent. $V_{TETA}:V_{H_2O}=1:1$. $[CoCl_2]=[TAA]=0.04\ mol\,L^{-1}$. a,b) lower magnification; c,d) higher magnification.

Results and Discussion

Synthesis of hollow hierarchical Co_9S_8 microspheres in a binary solution: Hierarchical hollow Co_9S_8 microspheres can be synthesized directly by a simple solvothermal process in a binary solution. The X-ray diffraction (XRD) pattern of as-prepared Co_9S_8 microspheres is shown in Figure 1. The

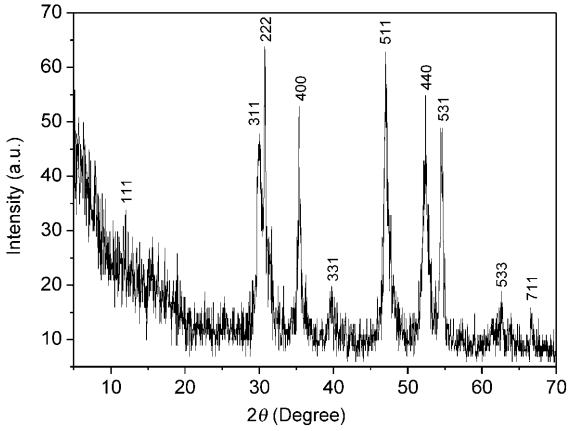

Figure 1. XRD pattern of Co_9S_8 hollow microspheres prepared by a solvothermal reaction in a mixed solvent at 180 °C for 12 h. $[CoCl_2]=[TAA]=0.04\ mol\,L^{-1}$, $V_{TETA}:V_{DIW}=1:1$.

strong and sharp diffraction peaks in the XRD pattern indicate that the obtained products are well crystallized. All the reflection peaks can be indexed to a pure cubic phase of Co_9S_8 with a lattice parameter of $a=9.907$ Å, which is consistent with the reported values (Joint Committee on Powder Diffraction Standards (JCPDS), Powder Diffraction File No: 86-2273).

The lower magnification of the SEM images in Figure 2 a,b show that a typical sample is composed of abundant hollow Co_9S_8 microspheres, which maintain a well-preserved spherical morphology with a diameters of ≈10–12 μm. A typical microsphere is shown in the magnified SEM image in Figure 2 c, and more details can be found in Figure 2 d, which demonstrate that the exterior of each hollow microsphere is composed of abundant randomly assembled quasi-hexagonal nanoplates, as well as loose and porous interiors.

The nanostructure of the Co_9S_8 quasi-hexagonal nanoplates obtained by sonication of the Co_9S_8 hollow microspheres was further investigated by TEM and high-resolution TEM (HRTEM). As shown in Figure 3 a,b, some quasi-

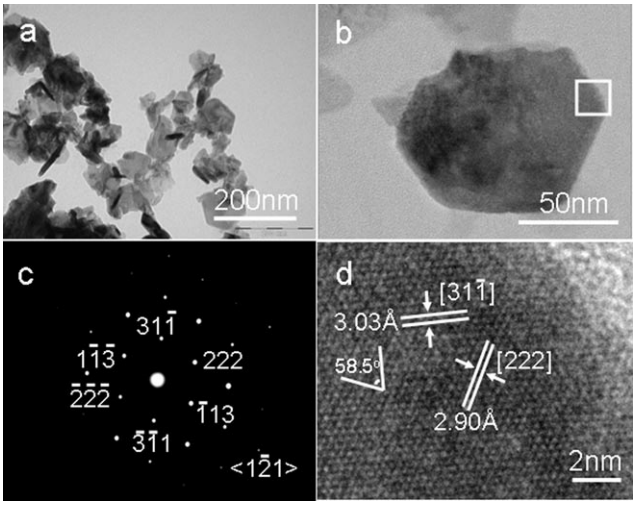

Figure 3. a) TEM image of quasi-hexagonal Co_9S_8 nanoplates; b) a typical quasi-hexagonal plate. c) Selected area electron diffraction pattern and d) an HRTEM image taken on a typical Co_9S_8 nanoplate marked by the white rectangle in b). The sample was prepared by a solvothermal reaction in a mixed solvent at 180 °C for 12 h, $V_{TETA}:V_{H_2O}=1:1$. $[CoCl_2]=[TAA]=0.04\ mol\,L^{-1}$.

hexagonal nanoplates with a size of ≈100 nm can be observed. Figure 3c shows the select area electron diffraction (SAED) pattern taken along the [1$\bar{2}$1] zone axis from part of such a Co_9S_8 nanoplate labeled by the white rectangle in Figure 3b, which shows the face-centered Co_9S_8 phase and single-crystalline nature of the Co_9S_8 nanoplate. The enlarged lattice-resolved HRTEM image shown in Figure 3d (the area marked by the white rectangle in Figure 3b) indicates that the spacing of the observed lattice planes are approximately 3.03 and 2.93 Å, which are consistent with the spacings for the (31$\bar{1}$) and (222) planes of cobalt pentlandite, respectively. The angle between (31$\bar{1}$) and (222) is 58.5°, which is consistent with that calculated for the face-centered structural formula.

The field emission SEM (FESEM) image of Co_9S_8 hollow microspheres in Figure 2d shows that the sample was composed of quasi-hexagonal highly crystalline plates, which indicates that the quasi-hexagonal nanoplates are stable in such a binary solution. The high resolution TEM image in Figure 3b shows a typical quasi-hexagonal plate. It is assumed that the formation of these quasi-hexagonal nanoplates is related to the intrinsic structural symmetry and atom stacking on the special plane surface. Figure 4a shows

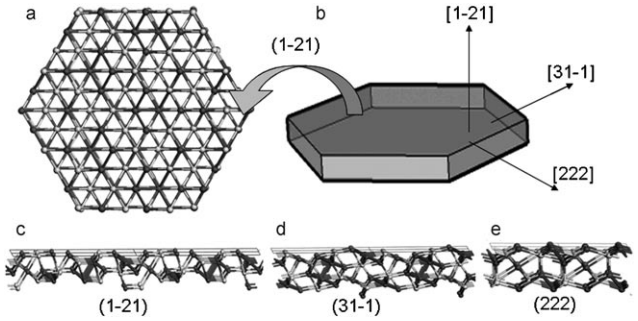

Figure 4. The structure and geometry model of Co_9S_8 quasi-hexagonal plate. a) a structure model view toward the (1$\bar{2}$1) plane; b) geometry model of Co_9S_8 hexagonal plate; c,d,e) structure models viewed along (1$\bar{2}$1), (31$\bar{1}$), and (222) respectively. Grey: Co atom, White: S atom.

the structural model viewed toward the (1$\bar{2}$1) plane, and illustrates the intrinsic hexagonal symmetry of Co_9S_8, which determines the formation of quasi-hexagonally symmetric nanoplates. Moreover, the atom stacking on the (1$\bar{2}$1), (31$\bar{1}$), and (222) plane surfaces were checked, and are shown in Figure 4c, d, and e, respectively. The stacking models on the (31$\bar{1}$) and (222) plane surfaces with Co atoms on the surface only are similar to each other, but totally different from the stacking model on the (1$\bar{2}$1) plane surface, in which the S atoms and Co atoms are located on the same surface. This is believed to induce a different surface energy of these planes, and it is assumed that the (1$\bar{2}$1) plane is more stable than the (31$\bar{1}$) and (222) planes, finally resulting in the formation of 2D platelike particles.

The XPS spectrum in Figure 5a indicates that the main peak values at 161.25, 284.6, 531.12, and 777.93 eV can be

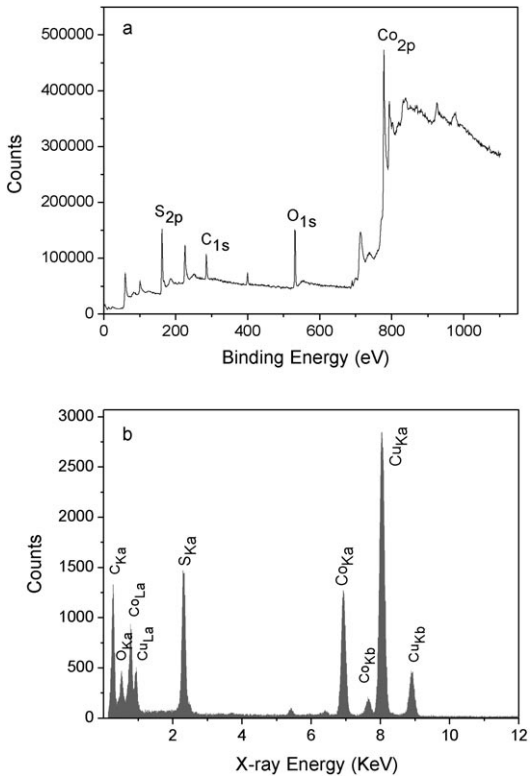

Figure 5. a) XPS and b) EDS spectra of the obtained Co_9S_8 hollow microspheres. The sample was prepared by a solvothermal reaction in a mixed solvent at 180°C for 12 h, $V_{TETA}:V_{H_2O}=1:1$. $[CoCl_2]=[TAA]=0.04\ mol\,L^{-1}$.

assigned readily to the binding energies of S_{2p}, C_{1s}, O_{1s}, and Co_{2p}, respectively. Quantitative analysis of the sample gives Co and S molar contents of 31.55 and 24.04%, respectively. The O element could be attributed to the surface adsorption of O_2 or slight surface oxidation of the obtained product exposed in air. Energy dispersive spectrum (EDS) analysis, shown in Figure 5b, indicates that the molar ratio of Co:S is 9:8.13. Therefore, both the XPS and EDS results confirm that the self-assembled hierarchical hollow microspheres are composed of pure phase Co_9S_8.

The nitrogen adsorption–desorption isotherms are measured to determine the specific surface area and pore volume of as-prepared Co_9S_8 hollow microspheres, and the corresponding results are presented in Figure 6. The pore size distribution, derived from desorption data and calculated from the isotherm using the BJH model, indicates that the average pores of such a sample are around 9.2 nm. The Brunauer–Emmett–Teller (BET) specific surface area of the sample calculated from N_2 adsorption is $80.38\ m^2\,g^{-1}$, which is much larger than those of usually prepared metal sulfides.[24] The much higher BET surface area of the hollow spheres may provide the possibility of efficient transport of electrons in lithium ion batteries.

A series of time-dependent experiments were performed in order to understand the formation process of novel hollow Co_9S_8 microspheres. The products obtained after re-

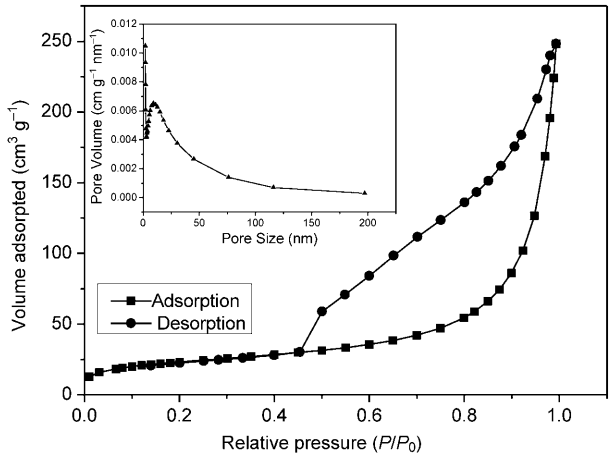

Figure 6. N_2 adsorption–desorption isotherm curve and pore size distribution (insert) of Co_9S_8 hollow microspheres. The sample was prepared by a solvothermal reaction in a mixed solvent at 180 °C for 12 h, V_{TETA}:V_{H_2O} = 1:1. [$CoCl_2$] = [TAA] = 0.04 mol L^{-1}.

action for different time intervals have been examined by XRD (see Supporting Information Figure S1). Figure 7 shows the FESEM images of the obtained sample from reaction for 1 h, 6 h, and 12 h, respectively. The microspheres with smaller diameters and rough surfaces formed after reaction of the mixture for 1 h (Figure 7a,b), and the TEM image shows that the particles are solid microspheres (see Supporting Information Figure S2). After reaction for 6 h, rough microspheres with a core shell microstructure come into being (Figure 7c). Figure 7d shows the enlarged magnification image of an individual core-shell microsphere, which indicates that a big core is located in the interior of the microspheres. Finally, when the reaction time was further prolonged to 12 h, the cores in the center of the core-shell microspheres are evacuated completely, resulting in hollow structures with an open void and hexangular nanoplates standing on their surface (Figure 7e,f).

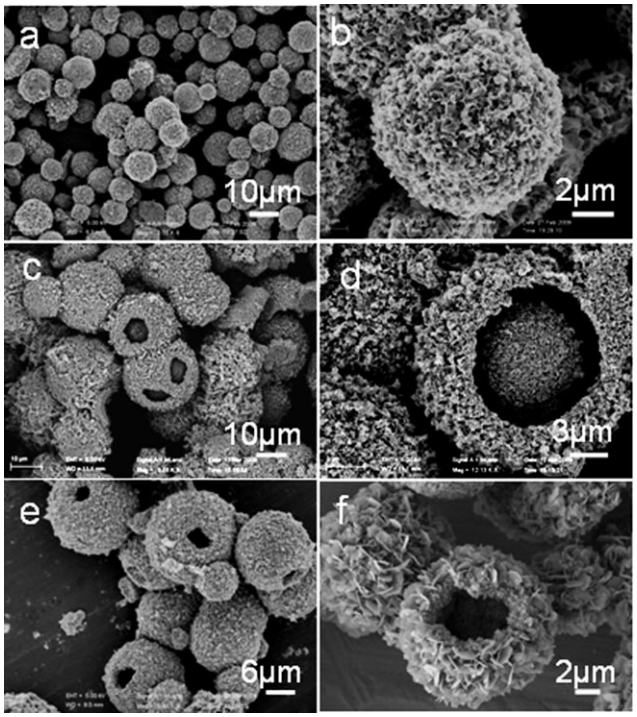

Figure 7. FESEM images of the samples prepared by a solvothermal reaction in a mixed solvent at 180 °C for different time periods. a,b) 1 h; c,d) 6 h; e, f) 12 h. V_{TETA}:V_{DIW} = 1:1. [$CoCl_2$] = [TAA] = 0.04 mol L^{-1}.

As the volume ratio of TETA:DIW (V_{TETA}:V_{DIW}) was varied, the shape of the particles and their microstructures changed. Randomly aggregated nanoplates were obtained when V_{TETA}:V_{DIW} was increased to 5:1 (Figure 8a), flower-like Co_9S_8 microstructures with diameters of 5 μm assembled by hexangular nanoplates were prepared when the volume ratio of V_{TETA}:V_{DIW} was increased to 2:1 (Figure 8b), and solid microspheres with rough surface and a diameter of ≈7 μm were produced when V_{TETA}:V_{DIW} decreased to 1:2 (Figure 8c). Randomly aggregated nanoplates also formed when V_{TETA}: V_{DIW} was further decreased to 1:5 (Figure 8d). The XRD patterns of the obtained products show that the samples synthesized in the solutions of different composition were mainly composed of pure phase Co_9S_8 (see Supporting Information Figure S3).

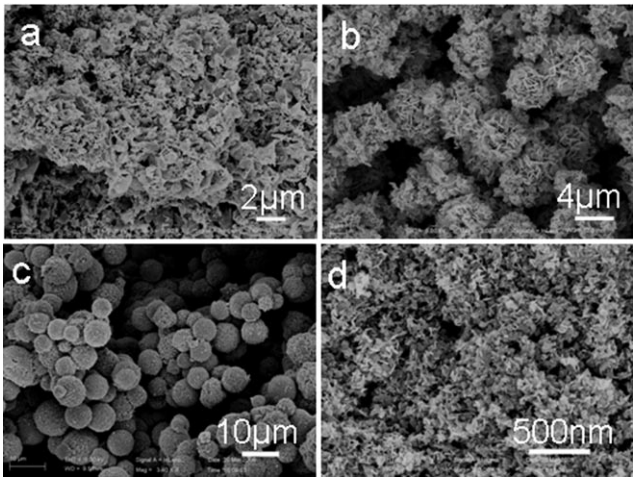

Figure 8. FESEM images of the samples prepared by a solvothermal reaction in a mixed solvent different volume ratios of V_{TETA}:V_{DIW} at 180 °C for 12 h. [$CoCl_2$] = [TAA] = 0.04 mol L^{-1}. a) 5:1; b) 2:1; c) 1:2; d) 1:5.

The influence of the volume ratio of TETA and DIW on the formation of Co_9S_8 particles with different microstructures may be due to the dissolution of TETA in DIW, while TETA was ionized by DIW ($TETA + H_2O \rightarrow TETAH^+ + OH^-$). The degree of ionization of TETA played an important role in the aggregation state of the processor and the morphology of the final product. The formation mechanism of such Co_9S_8 hollow microspheres obtained by a certain volume ratio of TETA and DIW in a binary solution could be attributed to the Ostwald ripening process, which has been commonly observed in general crystal growth many times, and involves the growth of larger crystals from those

of smaller size which have a higher solubility than the larger ones.[25] It has been reported that hierarchical hollow architectures such as Sn-doped TiO,[26] Cu_2O[27] $Cd(OH)_2$,[28] $CdMoO_4$,[29] and ZnS[30] can be prepared according to this classic Ostwald ripening process. In the present case, the evolution process of the Co_9S_8 hollow microspheres shows that the Ostwald ripening process is associated with a progressive redistribution of matter from the interior to the exterior of the microspheres. At the initial reaction stage, amorphous solid microspheres with a rough surface assembled by thin nanosheets were formed first after reaction for 1 h (step 1, Scheme 1). The exteriors of the newly formed

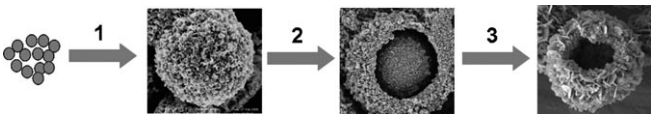

Scheme 1. Illustration of the formation process of the Co_9S_8 hollow microspheres.

solid microspheres were packed much more loosely than the interior, which indicates that the intrinsic density varies inside these microspheres,[26] and the nanobuilding blocks in the interior parts are smaller than those on the exterior.[31] Thus, the interior parts of the microspheres dissolved gradually, and the exterior loosely-packed nanosheets would serve as starting growth sites in the subsequent recrystallization stage. With the prolongation of the reaction, a reconstructing process occurs between the core and the shell, resulting in the formation of core-shell Co_9S_8 microspheres, with a core in their interior space and much thicker quasi-hexangular nanoplates standing on the exterior space (step 2, Scheme 1). Once the interior parts are dissolved completely, hollow microspheres with more uniform and thicker quasi-hexangular nanoplates, assembled on the outer surface, form through the Ostwald ripening mechanism (step 3, Scheme 1).

Magnetic properties of hollow hierarchical Co_9S_8 microspheres: The magnetization curve of the Co_9S_8 hollow microspheres at room temperature shows a paramagnetic property (Figure 9a). The temperature dependences of magnetization of the Co_9S_8 hollow microspheres under zero-field-cooled (ZFC) and field-cooled (FC) conditions are shown in Figure 9b; these indicate that there were nearly the same transferring trends between the ZFC and FC curves with the temperature changing at a magnetic field of 100 Oe, and also that the main paramagnetic properties of the obtained product occur at much higher temperature.[32]

The temperature (T) dependences of the molar magnetic susceptibility (χ) and the molar reciprocal magnetic susceptibility (χ^{-1}) are shown in Figure 10a and b. It was found that no anomaly is observed down to 4 K in the χ–T curve, and the magnetic susceptibilities obey the Curie–Weiss law above 150 K. Therefore, from the Curie–Weiss law fitting to

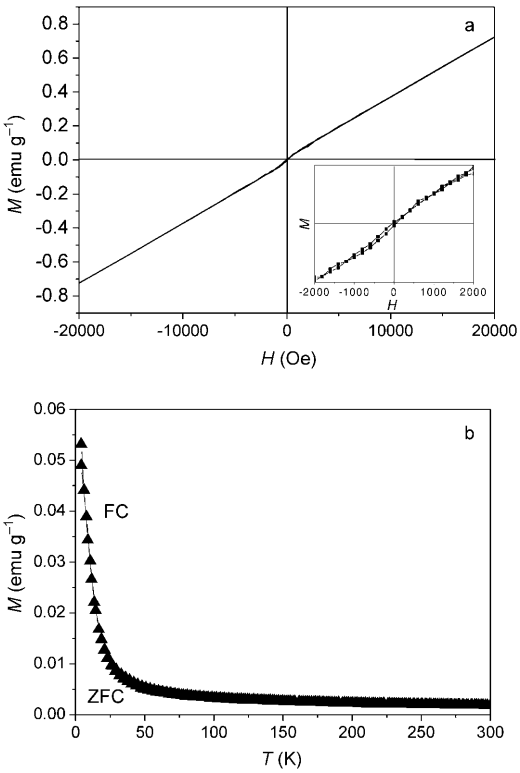

Figure 9. a) M–H curve at room temperature, and b) temperature dependence of magnetization measured at an applied field of 100 Oe for Co_9S_8 hollow microspheres under FC and ZFC processes. The sample was prepared by a solvothermal reaction in a mixed solvent at 180 °C for 12 h, $V_{TETA}:V_{H_2O}=1:1$. $[CoCl_2]=[TAA]=0.04$ mol L^{-1}.

the χ^{-1}–T curves (Figure 10b), it can be found that the Curie constant (C) is 3.305 emu K mol^{-1} Co and the Weiss constant (Θ_w) is −231 K. The negative Θ_w value suggests that there may be weakly antiferromagnetic interactions between the magnetic Co ions at much lower temperature.[33]

Electrochemical and electrocatalytic properties of hollow hierarchical Co_9S_8 microspheres: Figure 11a shows typical polarization curves of the oxygen reduction reaction on the obtained Co_9S_8 hollow microspheres in O_2-saturated 0.5 M H_2SO_4 with a rotation speed of 1600 rpm. For the sake of reference, the corresponding results on Pt/C are also given in Figure 11b. Rotating disk electrode (RDE) measurements indicate that the onset potential of the Co_9S_8 sample is 0.88 V, which is comparable to the predicted value for Co_9S_8 (0.74 V) from theoretical simulation,[16] and shows the accordance between the experimental and theoretical values of the onset potential of Co_9S_8 sulfide. However, the electrocatalytic activity of the sample toward the oxygen reduction reaction is much lower than that of Pt/C;[34] much effort needs to be devoted in the future to further improving its electrocatalytic activity toward the oxygen reduction reaction. Furthermore, it has to be pointed out that Co_9S_8 is much cheaper than Pt/C, it can still be used as a potential ORR electrocatalyst with higher currents[32] or higher current densities.[35]

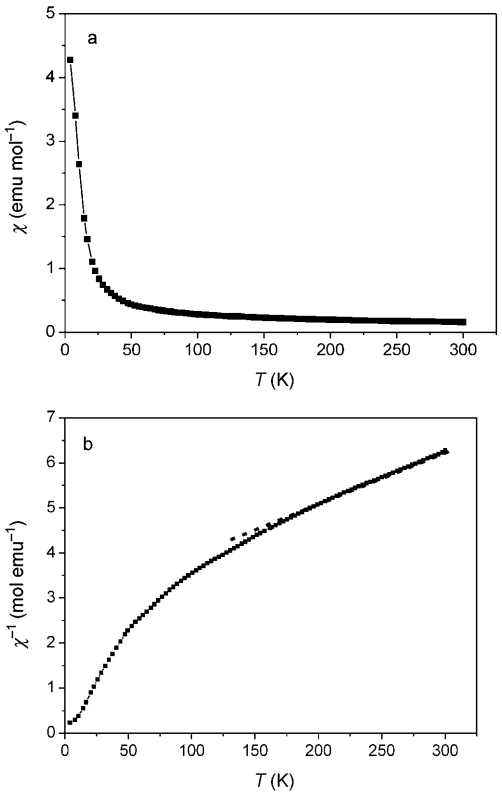

Figure 10. a) Temperature dependence of the magnetic susceptibilities of the χ–T curve, and b) the reciprocal susceptibilities with their fits to the Curie–Weiss law (short-dashed straight line) curve. The sample was prepared by a solvothermal reaction in a mixed solvent at 180 °C for 12 h, V_{TETA}:V_{H_2O} = 1:1. $[CoCl_2]$ = [TAA] = 0.04 mol L^{-1}.

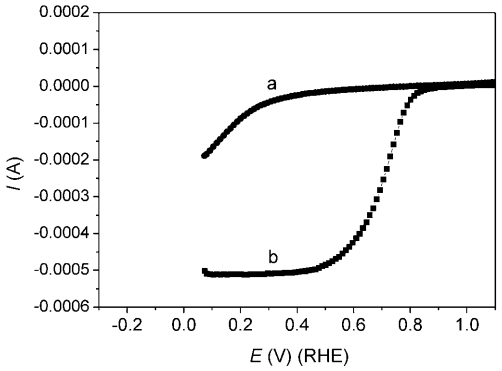

Figure 11. Current–potential curves of a) Co_9S_8 hollow spheres, and b) Pt/C for the O_2 reduction reaction. The sample was prepared by a solvothermal reaction in a mixed solvent at 180 °C for 12 h, V_{TETA}:V_{H_2O} = 1:1. $[CoCl_2]$ = [TAA] = 0.04 mol L^{-1}.

Due to the potential application of cobalt sulfide as the cathode material of lithium ion batteries, the charge and discharge capabilities of nanosized Co_9S_8[19] and CoS_2[36] have been reported and studied recently. However, the electrochemical properties of the hierarchical Co_9S_8 hollow microspheres have not yet been reported. Figure 12a shows the first three discharge and charge curves of the Co_9S_8 hollow

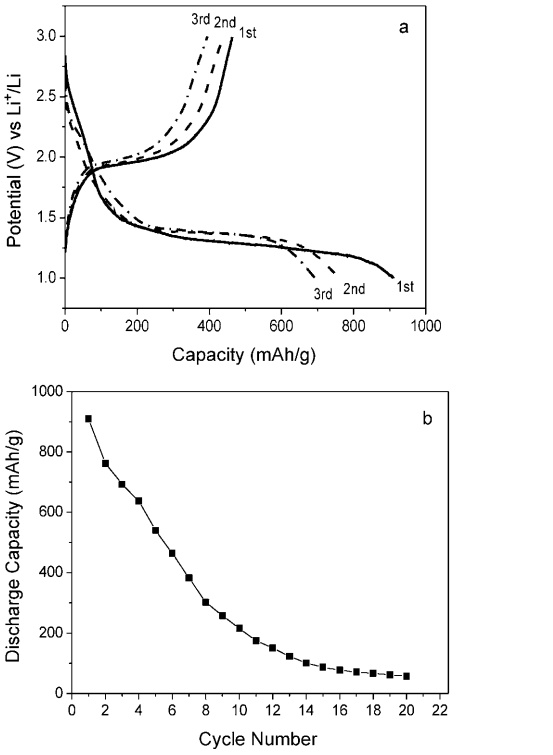

Figure 12. a) The first three discharge and charge curves of the Co_9S_8 hollow spheres. b) The curves of discharge capacities of Co_9S_8 hollow microspheres as cathode electrodes in Li cells versus the cycle number. The sample was prepared by a solvothermal reaction in a mixed solvent at 180 °C for 12 h, V_{TETA}:V_{H_2O} = 1:1. $[CoCl_2]$ = [TAA] = 0.04 mol L^{-1}.

spheres with capacities of 910.4, 762.3, and 692.8 mA h g^{-1}, respectively. Figure 12b presents a typical curve of the discharge capacity versus the cycle number for cells made from Co_9S_8 hollow microstructures, and shows that the initial five charge and discharge capacities are higher than the theoretical capacity (539 mA h g^{-1})[36] and capacities of Co_9S_8 nanoparticles.[36] Therefore, it was speculated that the larger surface area of the Co_9S_8 hollow spheres could play a role here. However, the cycle of charge and discharge capacities of such a sample is not stable because the discharge capacity dropped to 57.37 mA h g^{-1} after the 20th cycle. An irreversible capacity evidently exists, resulting from the irreversible reduction of Co from high valence state to low valence state indicated by the plateau at about 1.38 V, as well as the breakdown of the sulfide phases, and some side reactions with the electrolytes during the first reduction process as reported previously in the case of SnP_2O_7.[37] The electrochemical performance and the stability of the discharge capacity of Co_9S_8 hollow microspheres needs to be improved in the future.

Conclusion

In summary, hierarchical hollow Co_9S_8 microspheres have been synthesized by a simple solvothermal route in a binary

solution of triethylenetetramine (TETA) and deionized water (DIW). The Co_9S_8 hollow microspheres display dominant paramagnetic properties at higher temperature and weakly anti-ferromagnetic properties at lower temperature. The oxygen reduction reaction experiments show that the onset potential of the Co_9S_8 sample is 0.88 V, which is comparable to the predicted value for Co_9S_8 (0.74 V) from the theoretical simulation,[16] indicating the potential application of the as-prepared Co_9S_8 hollow microspheres as cheaper electrocatalysts. The discharge capacity of hollow Co_9S_8 microspheres at the initial discharge stage as lithium ion battery cathode materials is higher than that of the Co_9S_8 nanoparticles,[19] even though the cycle of charge and discharge capacities of such a sample is not stable, and requires more in-depth work for its improvement in the future.

Experimental Section

Synthesis of hierarchically self-assembled Co_9S_8 hollow microspheres: All reagents were of analytic grade and received from Shanghai Chemical Reagent Factory and used as received without purification. In a typical experiment, $CoCl_2 \cdot 6H_2O$ (1 mmol) and thioacetamide (C_2H_5NS, 1 mmol) were added into a mixed solvent of TETA and DIW with different volume ratio, with non-stop stirring. The solution was transferred into a Teflon-lined autoclave (with filling volume ratio of 80%) with a capacity volume of 30 mL after being stirred vigorously for about 30 min. The autoclave was closed and heated in a digital-type temperature-controlled oven at 180°C for 12 h, then cooled to room temperature naturally. The obtained products were filtered out and washed with absolute ethanol and distilled water.

Characterization: The obtained samples were characterized on a Philips X'Pert Pro Super X-Ray powder diffractometer with $Cu_{K\alpha}$ radiation ($\lambda = 1.541874$ Å). The morphology was examined with a JEOL JSM-6700F scanning electron microscope (SEM), and a Hitachi (Tokyo, Japan) H-800 transmission electron microscope (TEM) at an accelerating voltage of 200 kV, and a high-resolution transmission electron microscope (HRTEM) (JEOL-2010) operated at an acceleration voltage of 200 kV. Energy-dispersive X-ray (EDX) analysis was obtained with an EDAX detector installed on the same HRTEM. The X-ray photoelectron spectra (XPS) were collected on an ESCALab MKII X-ray photoelectron spectrometer, using non-monochromatized $Mg_{K\alpha}$ radiation as the excitation source. The surface area was calculated using the Brunauer–Emmett–Teller (BET) equation. Pore size distributions were calculated by the Barrett–Joyner–Halenda (BJH) method.

Magnetic properties measurement: The magnetic measurements on powder samples enclosed in a medical cap were carried out with a commercial superconducting quantum interference device (SQUID) magnetometer (MPMS-XL, Quantum Design Corp). The magnetization was measured under both zero field cooling (ZFC) and field cooling (FC) processes from 4 to 300 K, under an applied field of 100 Oe.

Electrochemical measurement: The working electrodes were made by mixing Co_9S_8 hollow microspheres (60 wt%), acetylene black (30 wt%), and polyvinylidene fluoride (PVDF; 10 wt%) binder in 1-methy l-2-pyrrolidinone (NMP) solvent to form a homogenous slurry. After ball-milling for 3 h at a rotation rate of 500 rpm, the working electrodes were obtained. The slurries were spread on copper foil substrates, and the coated electrodes were pressed after being dried in a vacuum oven at 100°C for 20 h. The cells were assembled with the working electrode as prepared, lithium metal as counterelectrode, and Celgard 2400 film as separator. The electrolyte was 1 M $LiPF_6$ in a mixture of ethylene carbonate (EC) and dimethyl carbonate (DMC) (1:1, v/v). Cell assembly was carried out in an argon-filled glove box (M Braun 100 G, Germany), where the water and oxygen concentration was kept less than 1 ppm. The cells were galvanostatically charged and discharged at a current density of 50 mA g^{-1} between 0.02 and 3.0 V. The specific capacities were calculated based on the total weight of electrode materials.

Electrocatalytic property measurement: Rotating disk electrode (RDE) measurements were performed in a three-electrode electrochemical cell at room temperature. A glassy carbon disk (5.0 mm diameter) was employed as the working electrode. A catalyst ink was prepared by mixing the as-prepared Co_9S_8 catalyst powder with isopropyl alcohol in an ultrasonic bath. The obtained well-dispersed catalyst ink was deposited on the glassy carbon disk until a total catalyst loading of 610 μg cm^{-2} was achieved. After drying, 10 μL of a mixture of Nafion solution (5 wt%, Aldrich) and isopropyl alcohol was coated onto the catalyst layer to ensure better adhesion of the catalyst on the glassy carbon substrate. An aqueous solution of 0.5 M H_2SO_4 was used for the electrolyte, and Platinum mesh and $Hg/HgSO_4$ electrodes were used as the counter and reference electrodes, respectively. All potentials in this work are referred to the normal hydrogen electrode (NHE) scale. The electrocatalytic activity for oxygen reduction was evaluated in the oxygen-saturated electrolyte.

Acknowledgements

S.H.Y. acknowledges the funding support from the National Basic Research Program of China (2010CB934700), the Program of International S & T Cooperation (2010DFA41170), and the National Natural Science Foundation of China (No. 50732006), and the Principle Investigator Award from the National Synchrotron Radiation Laboratory (NSRL, Hefei, China).

[1] a) D. Chen, J. H. Ye, *Adv. Funct. Mater.* **2008**, *18*, 1; b) W. M. Zhang, J. S. Hu, Y. G. Guo, S. F. Zheng, L. S. Zhong, W. G. Song, L. J. Wan, *Adv. Mater.* **2008**, *20*, 1160; c) H. S. Im, U. Jeong, Y. N. Xia, *Nat. Mater.* **2005**, *4*, 671; d) A. Bigi, E. Boanini, D. Walsh, S. Mann, *Angew. Chem.* **2002**, *114*, 2267; *Angew. Chem. Int. Ed.* **2002**, *41*, 2163; e) H. C. Zeng, *J. Mater. Chem.* **2006**, *16*, 649; f) J. B. Fei, Y. Cui, X. H. Yan, W. Qi, Y. Yang, K. W. Wang, Q. He, J. B. Li, *Adv. Mater.* **2008**, *20*, 452; g) Q. Zhang, W. S. Wang, J. Goebl, Y. D. Yin, *Nano Today* **2009**, *4*, 494.

[2] a) H. T. Schmidt, A. E. Ostafin, *Adv. Mater.* **2002**, *14*, 532; b) D. H. W. Hubert, M. Jung, A. L. German, *Adv. Mater.* **2000**, *12*, 1291; c) Y. R. Ma, L. M. Qi, J. M. Ma, H. M. Cheng, *Langmuir* **2003**, *19*, 4040.

[3] a) H. G. Yang, H. C. Zeng, *Angew. Chem.* **2004**, *116*, 5318; *Angew. Chem. Int. Ed.* **2004**, *43*, 5206; b) Y. Li, J. Shi, Z. Hua, H. Che, M. Ruan, D. Yan, *Nano Lett.* **2003**, *3*, 609; c) C. E. Fowler, D. Khushalani, S. Mann, *Chem. Commun.* **2001**, 2028.

[4] Q. Peng, Y. J. Dong, Y. D. Li, *Angew. Chem.* **2003**, *115*, 3135; *Angew. Chem. Int. Ed.* **2003**, *42*, 3027.

[5] a) J. B. Jackson, N. J. Halas, *J. Phys. Chem. B* **2001**, *105*, 2743; b) K. P. Velikov, A. V. Blaaderen, *Langmuir* **2001**, *17*, 4779; c) Y. Wang, F. B. Su, J. Y. Lee, X. S. Zhao, *Chem. Mater.* **2006**, *18*, 1347; d) V. Salgueiriño-Maceira, M. Spasova, M. Farle, *Adv. Funct. Mater.* **2005**, *15*, 1036.

[6] a) F. Caruso, P. A. Caruso, H. Mőhwald, *Science* **1998**, *282*, 1111; b) F. Caruso, X. Shi, P. A. Caruso, A. Susan, *Adv. Mater.* **2001**, *13*, 740; c) D. G. Shchukin, R. A. Caruso, *Chem. Mater.* **2004**, *16*, 2287.

[7] A. B. Bourlinos, M. A. Karakassides, D. Petridis, *Chem. Commun.* **2001**, 1518.

[8] a) A. G. Dong, N. Ren, Y. Tang, *J. Am. Chem. Soc.* **2003**, *125*, 4976; b) Y. D. Xia, M. Robert, *J. Mater. Chem.* **2005**, *15*, 3126; c) M.-M. Titirici, M. Antonietti, A. Thomas, *Chem. Mater.* **2006**, *18*, 3808.

[9] Y. D. Yin, R. M. Rioux, C. K. Erdonmez, S. Hughes, G. A. Somorjai, A. P. Alivisatos, *Science* **2004**, *304*, 711.

[10] H. G. Yang, H. C. Zeng, *J. Phys. Chem. B* **2004**, *108*, 3492.

[11] a) J. G. Yu, H. Guo, S. A. Davis, S. Mann, *Adv. Funct. Mater.* **2006**, *16*, 2035; b) H. Li, Z. Bian, J. Zhu, D. Zhang, G. Li, Y. Huo, H. Li, Y. Lu, *J. Am. Chem. Soc.* **2007**, *129*, 8406.

[12] J. Yang, L. M. Qi, C. Lu, J. M. Ma, H. M. Cheng, *Angew. Chem.* **2005**, *117*, 604; *Angew. Chem. Int. Ed.* **2005**, *44*, 598.
[13] X. L. Yu, C. B. Cao, H. S. Zhu, Q. S. Li, C. L. Liu, Q. H. Gong, *Adv. Funct. Mater.* **2007**, *17*, 1397.
[14] a) N. Kamoun, S. Belgacem, M. Amlouk, and R. Bennaceur, *J. Appl. Phys.* **2001**, *89*, 2766; b) H. F. Bao, C. M. Li, X. Q. Cui, Q. L. Song, H. B. Yang, J. Guo, *Nanotechnology* **2008**, *19*, 335302; c) H. F. Bao, C. M. Li, X. Q. Cui, Y. Gan, Q. L. Song, J. Guo, *Small* **2008**, *4*, 1125.
[15] a) S . Takele1, G. R. Hearne, *J. Phys. Condens. Matter* **2001**, *13*, 10077; b) S. J. Bao, Y. B. Li, C. M. Li, Q. L. Bao, Q. Lu, J. Guo, *Cryst. Growth Des.* **2008**, *8*, 3745.
[16] R. A. Sidik, A. B. Anderson, *J. Phys. Chem. B* **2006**, *110*, 936.
[17] a) T. Kadono, T. Kubota, I. Hiromitsu, Y. Okamoto, *Appl. Catal A* **2006**, *312*, 125; b) D. M. Pasquariello, R. Kershaw, J. D. Passaretti, K. Dwight, A. Wold, *Inorg. Chem.* **1984**, *23*, 872; c) I. Bezverkhyy, P. Afanasiev, M. Danot, *J. Phys. Chem. B* **2004**, *108*, 7709.
[18] a) D. Baresel, W. Sarholz, P. Scharner and J. Schmitz, *Ber. Bunsen-Ges.* **1974**, *78*, 608; b) H. Behret, H. Binder and G. Sandstede, *Electrochim. Acta* **1975**, *20*, 111.
[19] a) J. Wang, S. H. Ng, J . Chen, L. Zhao, Y. Chen, H. K. Liu, *J. Power Sources* **2006**, *159*, 287; b) R. D. Apostolova, E. M. Shembel, I. Talyosef, J. Grinblat, B. Markovsky, D. Aurbach, *Russ. J. Electrochem.* **2009**, *45*, 311.
[20] P. F. Yin, L. L. Sun, Y. L. Gao, S. Y. Wang, *Bull. Mater. Sci.* **2008**, *31*, 593.
[21] a) C. Wang, X. M. Zhang, X. F. Qian, Y. Xie, Y. T. Qian, *J. Phys. Chem. Solids* **1999**, *60*, 2005; b) X. F. Qian, X. M. Zhang, C. Wang, Y. Xie, Y. T. Qian, *Inorg. Chem.* **1999**, *38*, 2621; c) X. H. Liu, *Mater. Sci. Eng. B* **2005**, *119*, 19.
[22] Y. D. Yin, C. K. Erdonmez, A. Cabot, S. Hughes, A. P. Alivisatos, *Adv. Funct. Mater.* **2006**, *16*, 1389.
[23] W. T. Yao, S. H. Yu, *Adv. Funct. Mater.* **2008**, *18*, 3357.
[24] a) W. T. Yao, S. H. Yu, S. J. Liu, J. P. Chen, X. M. Liu, F. Q. Li, *J. Phys. Chem. B* **2006**, *110*, 11704; b) Z. H. Han, H. Y. Zhu, J. Shi, G. Parkinsona, G. Q. Lu, *J. Solid State Chem.* **2007**, *180*, 902.
[25] W. Z. Ostwald, *Phys. Chem.* **1900**, *34*, 495.
[26] J. Li, H. C. Zeng, *J. Am. Chem. Soc.* **2007**, *129*, 15839.
[27] Y. Chang, J. J. Teo, H. C. Zeng, *Langmuir* **2005**, *21*, 1074.
[28] W. S. Wang, L. Zhen, C. Y. Xu, W. Z. Shao, *J. Phys. Chem. C* **2008**, *112*, 14360.
[29] W. S. Wang, L. Zhen, C. Y. Xu, B. Y. Zhang, W. Z. Shao, *J. Phys. Chem. B* **2006**, *110*, 23154.
[30] B. Liu, H. C. Zeng, *Small* **2005**, *1*, 566.
[31] Y. X. Gao, S. H. Yu, H. P. Cong, J. Jiang, A. W. Xu, W. F. Dong, H. Cölfen, *J. Phys. Chem. B* **2006**, *110*, 6432–6436.
[32] S. Ferdov, A. M. L. Lopes, Z. Lin, R. A. SáFerreira, *Chem. Mater.* **2007**, *19*, 6025.
[33] Y. Matsushita, Y. Ueda, *Inorg. Chem.* **2006**, *45*, 2022.
[34] E. Vayner, R. A. Sidik, A. B. Anderson, *J. Phys. Chem. C* **2007**, *111*, 10508.
[35] Y. J. Feng, T. He, N. Alonso-Vante, *Chem. Mater.* **2008**, *20*, 26.
[36] J. M. Yan, H. Z. Huang, J. Zhang, Z. J. Liu, Y. Yang, *J. Power Sources* **2005**, *146*, 264.
[37] Y. M. Li, J. H. Li, *J. Phys. Chem. C* **2008**, *112* , 14216.

Received: November 29, 2009
Revised: April 4, 2010
Published online: September 6, 2010

